

國立雲林科技大學  
100 學年度博士班招生考試試題

所別：化學工程與材料工程系

科目：科技文獻

一、根據附件一，回答下列問題：

1. 本篇論文的研究目的? (10%)
2. 本篇論文主要的實驗方法? (20%)
3. 本篇論文的具體貢獻? (20%)

二、根據附件二，回答下列問題：

4. 本篇論文的目的? (10%)
5. 本篇論文的研究方法? (20%)
6. 本篇論文的具體貢獻? (20%)



## Surface plasmon resonance biosensor for microalbumin detection

Jen-Tsai Liu<sup>a</sup>, Po-Shen Lin<sup>a</sup>, Yue-Ming Hsin<sup>b</sup>, Jang-Zern Tsai<sup>b</sup>, Wen-Yih Chen<sup>a,c,\*</sup>

<sup>a</sup> Department of Chemical and Materials Engineering, National Central University, Taoyuan 32001, Taiwan

<sup>b</sup> Department of Electrical Engineering, National Central University, Taoyuan 32001, Taiwan

<sup>c</sup> Center for Dynamical Biomarkers and Translational Medicine, National Central University, No.300, Jhongda Rd., Jhongli City, Taoyuan County 32001, Taiwan

### ARTICLE INFO

#### Article history:

Received 5 August 2010

Received in revised form 27 December 2010

Accepted 11 January 2011

#### Keywords:

Human serum albumin

Surface plasmon resonance

Cibacron Blue F3G-A

### ABSTRACT

Human serum albumin (HSA) is an important biomarker for diagnosing nephropathy. Traditional microalbumin detection is easily affected by the intake of certain medicines, such as aspirin, corticosteroids and antibiotics. In this research, the surface plasmon resonance (SPR) biosensor technique was used to detect HSA. The anthraquinone dye Cibacron Blue F3G-A (CB) is used as a receptor which has a specific affinity for HSA. The purpose of this study is establishing the optimum conditions for SPR to detect HSA. The results exhibited that the sensor chip has high affinity as well as high capacity at pH 4 with 0.05 M sodium chloride. In addition, linear response appeared in the range of 0.01–0.1 mg/ml HSA and the detecting limit was 4  $\mu$ g/ml. This methodology may prove to be useful in clinical diagnosis and may serve as an assay for HSA binding ability.

© 2011 Taiwan Institute of Chemical Engineers. Published by Elsevier B.V. All rights reserved.

### 1. Introduction

Human serum albumin (HSA) is commonly found in the blood and is filtered by the kidneys. If the kidneys are damaged, first symptom is small amounts of HSA will leak into the urine. It is called microalbuminuria. However, many other conditions can lead to kidney damage, such as high blood pressure, heart failure, cirrhosis, or systemic lupus erythematosus (SLE) (Lièvre *et al.*, 2000). Microalbumin is the earliest clinical symptom in renal disease, defined as 30–300 mg/dl of albumin in the urine (Pantelis and George, 2006; Spyridon *et al.*, 2005). In the early stage of kidney damage, treatment with angiotensin-converting enzyme (ACE) inhibitors and angiotensin receptor blockers (ARB) may prevent progression to overt proteinuria and end renal failure stage in patients (Lewis *et al.*, 2001). Therefore, regular screening to detect microalbumin is essential. Currently, HSA is usually measured by immunoturbidimetric assays (ITA) (Ottavio *et al.*, 1992). The ITA method is widely used to estimate the quantity of albumin present in urine. It is time-consuming and may be affected by the intake of certain medicines, such as aspirin, corticosteroids, and some antibiotics (Pagana and Pagana, 2006).

In this research, the surface plasmon resonance (SPR) biosensor technique was used to detect HSA. SPR is one of the most sensitive direct non-labeled optical sensing techniques for real-time monitoring of biological and chemical interactions (Chen *et al.*, 2005; Nan *et al.*, 2007; Ying *et al.*, 2007). The aim of this study is to develop a new method for detecting microalbumin, including

surface modification chemistry of the sensor chip. In addition, this study seeks to determine the optimum condition for detecting HSA.

### 2. Methods and materials

#### 2.1. Chemicals and reagents

Cibacron Blue F3GA (CB) was purchased from Acros Organics (USA), while (1-Mercaptooundec-11-yl)tetra(ethylene glycol) (PEG-thiol), lysozyme, and human serum albumin (HSA) were obtained from Sigma (USA). The pH of the adsorption buffer was varied between 3, 4, 5 and 7.4 using different buffer systems (0.1 M CH<sub>3</sub>COONa-/CH<sub>3</sub>COOH for pH 3.0, 4.0, 5.0; 0.1 M K<sub>2</sub>HPO<sub>4</sub>-/KH<sub>2</sub>PO<sub>4</sub> for pH 7.4), with each one containing different concentrations of sodium chloride (0 M, 0.05 M, and 0.15 M), respectively. Other reagents and solvents were purchased commercially and were used without further purification.

#### 2.2. Surface modification

##### 2.2.1. Chip fabrication

In this study, SF11 optical glass substrates were used as sensor chips and coated with 1 nm adhesion-promoting chromium layer and 47.5 nm surface plasmon active gold layer through thermal evaporation under vacuum.

##### 2.2.2. Preparation of self-assembled monolayer

A schematic diagram of the PEG-CB membrane surface modification procedures is shown in Fig. 1. A 0.2 mM ethylene glycol alkanethiol (PEG) was dissolved in absolute ethanol. The

\* Corresponding author. Tel.: +886 3 422 7151x34222; fax: +886 3 422 5258. E-mail address: [wychen@cc.ncu.edu.tw](mailto:wychen@cc.ncu.edu.tw) (W.-Y. Chen).

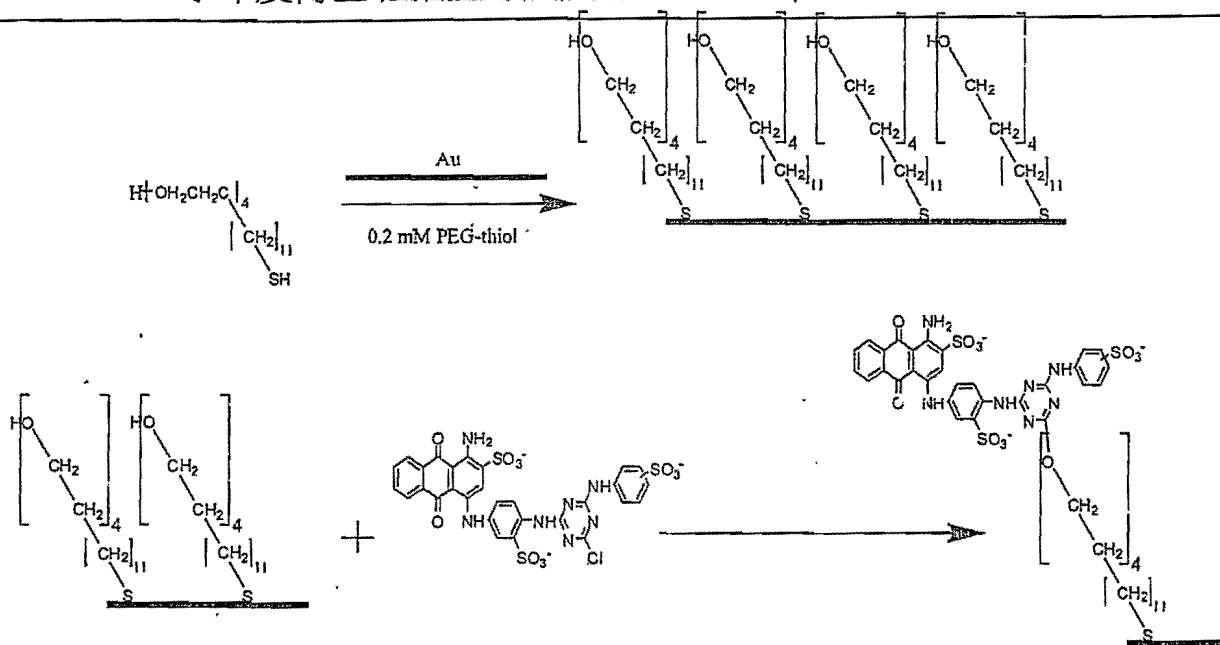


Fig. 1. Schematic diagram of the surface modification procedures of the PEG-CB membrane.

chips were then cleaned by UV-ozone for 20 min. Following UV cleaning, these chips were again exhaustively rinsed with water followed by absolute ethanol. The cleaned chips were immersed in the PEG solution described above overnight at 37 °C. Then, the modified chip was washed several times with absolute ethanol and dried under nitrogen.

### 2.2.3. CB immobilization

CB was immobilized on the PEG membranes via the nucleophilic reaction between the chloride of its triazine ring and the hydroxyl group of the PEG molecule under alkaline conditions (pH = 11). First, the PEG-modified chip was immersed in a 2 mM CB dye solution for 30 min at 60 °C in order to make CB dispersion on the chip surface well. After 30 min, an equal volume of Na<sub>2</sub>CO<sub>3</sub> aqueous solution (1 wt%) was added slowly to accelerate the nucleophilic reaction between the dye and the hydroxyl group of the PEG molecule, which took place for 4 h at 80 °C. Finally, the PEG-CB monolayer was washed with DI water. The immobilizing process was followed by the previously literatures (Altıntas and Denizli, 2006; Christina *et al.*, 2003; Handan *et al.*, 2003; Hua and Zhu, 2007; Shengfu *et al.*, 2000; Zuwei *et al.*, 2006).

### 2.3. Characterization of PEG-CB monolayer

The PEG-CB monolayer was characterized by contact angle and Electron Spectroscopy for Chemical Analysis (ESCA) (Thermo VG-Scientific, Sigma Probe) analyses. Contact angle is a preliminary metric for understanding material surface properties and the effects of surface treatments. ESCA is a quantitative spectroscopic technique that measures elemental composition.

### 2.4. SPR spectroscopic measurement

A home-built SPR biosensor (Chen *et al.*, 2005) based on the Kretschmann configuration using attenuated total reflection (ATR), combined with the flow analysis system, was used to monitor recognition interaction between PEG-CB monolayer and HSA. The sensor chip was attached to the prism base, and optical contact was established using a refractive index matching fluid ( $n = 1.778$ ).

A p-polarized light wave from 632.8 nm wavelength He-Ne laser, as a light source, is incident directly at an internal angle of  $\theta$  at the gold-prism interface. This SPR metrology system has an angular accuracy of 0.0001° and is capable of yielding precise analytical data. To obtain interaction measurements, the SPR was first stabilized in a carries buffer for 15 min. When the system reached a steady state, the sample (HSA) was injected for 30 min (flow rate 0.46  $\mu$ l/min). Then, the carries buffer was used for washing for a period of 30 min. Finally, 1 N NaOH was injected for 1 min for regeneration.

## 3. Results

### 3.1. Characterization of PEG-CB monolayer

Contact angle is a powerful technique for interpret the surface quality. The contact angle of bare Au was 69.7°. After forming the PEG monolayer, the contact angle was changed from 69.7° to 30.2°. The angle change was attributed to the OH functional group of PEG, which is more hydrophilic than a bare Au surface. When the CB was immobilized on PEG monolayer, the contact angle was changed from 30.2° to 34.6°. This change was not significant due to the ligand of CB, which contains three acidic sulfonate groups and four basic primary and secondary amino groups (Martins *et al.*, 2003). To verify whether or not CB was immobilized on the PEG surface, the ESCA was used to confirm the elements of chip surface. All SAMs were analyzed by ESCA. This technique was used to verify the presence of CB. The modification of the PEG surface with CB was corroborated by the presence of nitrogen in the region of 400 eV (Fig. 2(a)). Only one peak of nitrogen was found and was assigned to the nitrogen of the CB molecule. It can prove the CB was immobilized successfully. Fig. 2(b) illustrates the ESCA spectra of the S for SAMs with CB. The monolayer exhibits an RS<sup>-</sup> peak at 162 eV, which is a characteristic of thiolates on gold (David *et al.*, 1996). The other peak at 168 eV is associated with sulfur bound to three oxygen atoms (SO<sub>3</sub><sup>-</sup>). The existence of nitrogen and oxidized sulfur evidenced that the CB was immobilized on the PEG monolayer. According to the peak analysis, the peak area ratio of 168 eV and 162 eV was 0.18. It is obvious that the component of

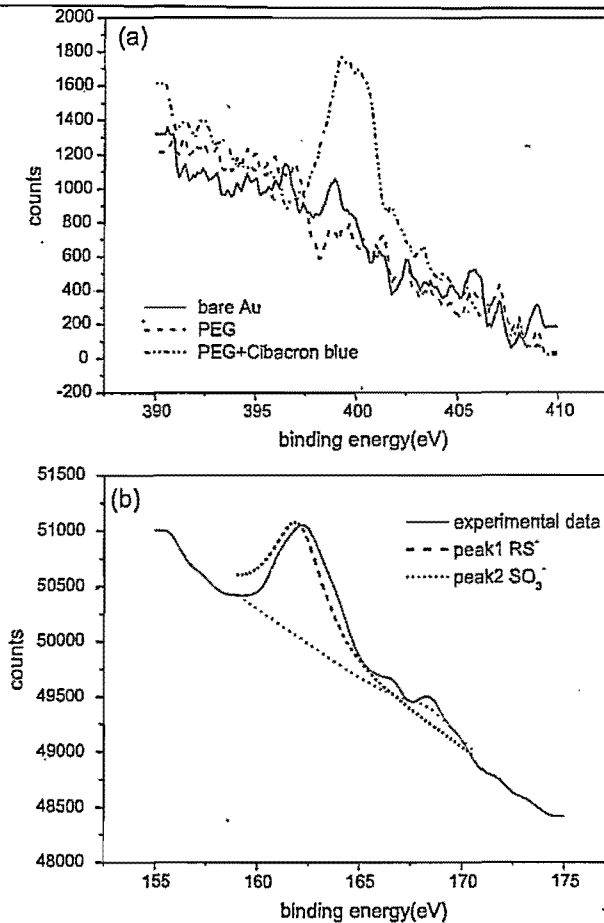


Fig. 2. ESCA for analyzing the PEG-CB monolayer on the sensor surface. (a) The element of N was significance after CB immobilization. (b) Quantitative analyzed of the PEG-thiol and CB.

PEG-CB is about 6%. The result is similar to previous literature (Martins *et al.*, 2003). Based on these results, we could assume that the HSA biosensor had fabricated successfully.

### 3.2. SPR spectroscopic measurement

To characterize the SPR system response, the lysozyme (0.1 mg/ml) was tested for non-specific adsorption corresponding to

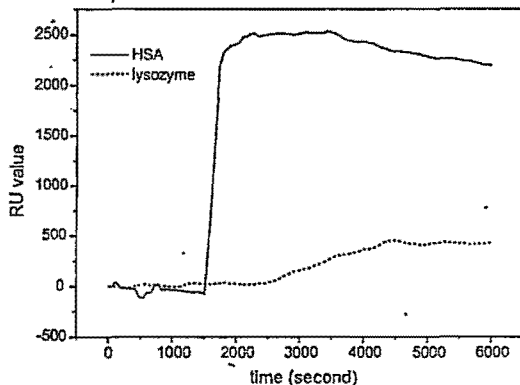


Fig. 3. To characterize the response of SPR system the lysozyme (0.1 mg/ml) was test for non-specific adsorption, corresponding to 0.1 mg/ml HSA followed by the PEG-CB monolayer.

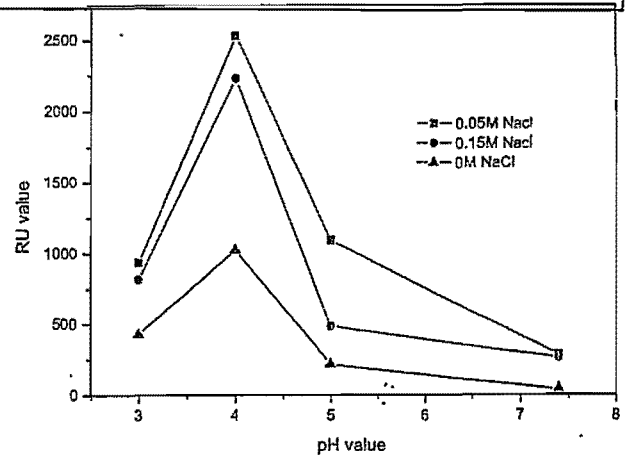


Fig. 4. The adsorption of the PEG-CB monolayer and the HSA spectrum of the four kinds of solutions, in different pH value and salt concentration.

0.1 mg/ml HSA, followed by the PEG-CB monolayer. The typical results of these experiments are presented in Fig. 3. The SPR signal gram obtained for two samples are easily distinguishable and the PEG-CB monolayer was highly specific to HSA.

Fig. 4 presents the dependence on the adsorption of the PEG-CB monolayer and the HSA spectrum with different solutions. These results indicate that pH of the binding solution could have an important effect on the adsorption equilibrium of HSA. The maximum signal change was observed at about 2500 resonance unit (R.U.) at pH 4. As the pH value changes from 5 to 7, the HSA adsorption decreased by about 67–80%. Furthermore, the SPR signal shift was decreased about 67–80% with decreasing pH value below 4. Therefore, pH is an important factor which influences recognition between HSA and CB.

The effects of ionic strength on HSA adsorption are also presented in Fig. 4. The effect of ionic strength was adjusted by using NaCl. The adsorption capacity increased with increasing ionic strength of the carry buffer. The adsorption of HSA increased about 50% as NaCl concentration increased from 0.05 to 0.15 M. The maximum signal change was observed at an ionic strength of 0.05 M. These results indicated that a buffer at pH 4 with a 0.05 M NaCl is optimum condition for detecting HSA.

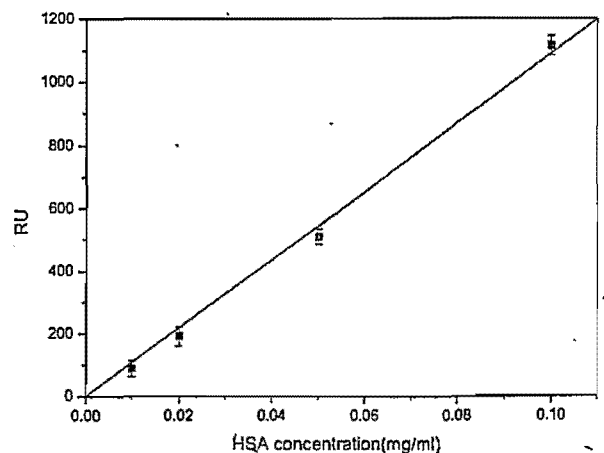


Fig. 5. Linear response to HSA in the range from 0.01 mg/ml to 0.1 mg/ml in 0.1 M acetic acid-sodium acetate buffer pH = 4, contains 0.05 M sodium chloride. There are four different concentrations; 0.01 mg/ml, 0.02 mg/ml, 0.05 mg/ml and 0.1 mg/ml.

### 3.3. Calibration and statistics evaluation of this method

From the above results, we can conclude that the best condition to detect HSA is 0.1 M acetic acid-sodium acetate buffer at pH 4 containing 0.05 M sodium chloride. To estimate the detectable range for clinical diagnosis application, we designed a concentration range of HSA between 0.01 and 0.1 mg/ml, which contains normal physiology range (lower 0.02 mg/ml) and microalbuminuria range (between 0.02 mg/ml and 0.1 mg/ml) (Spyridon *et al.*, 2005) for measurement. Fig. 5 shows the standard curve ( $n \geq 3$ ) of HSA. In the range of the experiments, the concentration of HSA and SPR signal exhibited a good linear fitting ( $R = 0.998$ ,  $P < 0.0001$ ). In our system, the detecting limit is 4  $\mu\text{g/ml}$ . The results show that the SPR system is sensible to investigate the changes in HSA concentration in a normal physiology and microalbuminuria range. Therefore, the SPR system has good potential for clinical diagnosis.

## 4. Discussion

### 4.1. The effect of pH

The range of the pH value studied covers the HSA's isoelectric point (pI), which is about 4.7–5.2. Based on the previous study (Galina and Dimo, 2006), the HSA structure is composed of three  $\alpha$ -helix domains, with each domain having its own charge characteristics. The possible active sites of CB which will allow it to react with the proteins are  $\text{SO}_3\text{H}$ ,  $\text{NH}_2$ , and  $\text{NH}$ . As the pKa of  $\text{SO}_3\text{H}$  is about 0.7–1.0, its reaction medium becomes negative, and as the pKa of  $\text{NH}_2$  and  $\text{NH}$  are between 7.7 and 11.7, the reaction medium with these active sites becomes positive (Sosnovsky and Bell, 1998; Stephan *et al.*, 2003).

Fig. 4 shows the effect of pH on the adsorption of HSA onto the PEG-CB monolayer. In all the investigated experiments, the maximum adsorption of HSA was observed at pH 4.0, which was near the isoelectric point of HSA. In addition, the net charge of HSA at this pH was close to zero. According to previously study, near the isoelectric point, the maximum protein adsorption was usually observed since the charge of HSA was closed to zero (Handan *et al.*, 2003). On the other hand, the minimum adsorption of HSA was observed at pH 7.4. At this pH, the HSA charge and the active sites of  $\text{SO}_3\text{H}$  in CB were both negative. Thus, the electrostatic interaction (long-term force) was repulsed and there was no possibility of forming a complex through hydrophobic interaction (short-term force). These results directed the electrostatic interaction was one of important factors could affect the binding process.

### 4.2. The effect of salt concentration

Electrostatic interaction is protected by the presence of ions. With respect to the composition of proteins, the polar and the non-polar regions are separated. Increasing the ionic strength could enhance the hydrophobic interaction because the electrostatic interaction is protected. The effect of ionic strength on HSA adsorption is illustrated in Fig. 4. It can be seen that the adsorption capacity rapidly increases at an ionic strength in 0.05 M. The increase in the adsorption capacity with increasing in the ionic strength can be attributed to the repulsive electrostatic interactions and enhance the hydrophobic interaction between the CB and the HSA. When the salt concentration increases in the adsorption buffer, the sulfonic acid groups of the CB binds with sodium ions, which could lead to low protein adsorption (Kassab *et al.*, 2000). However, in pH 4, the charge of HSA was closed to zero and the protein adsorption was usually observed by the hydrophobic interaction (Handan *et al.*, 2003).

The result indicates that adding salt could certainly affect the hydrophobic interaction. To compare the condition with 0.05 M salt and without salt, the SPR signal was actually increased by adding the salt. This showed that adding salt could raise hydrophobic force. This effect benefited the short-term force (hydrophobic force) and enhanced the HSA adsorption. This result also exhibited that the hydrophobic interaction was another one of important factors could affect the binding process.

## 5. Conclusion

This work demonstrates that SPR can successfully detect and quantify HSA binding to the PEG-CB monolayer through a specific interaction. The optimum condition for detecting HSA is 0.1 M acetic acid-sodium acetate buffer at pH 4 containing 0.05 M sodium chloride. The detecting linear response appeared in the range of 0.01–0.1 mg/ml HSA and the detecting limit is 4  $\mu\text{g/ml}$ . In addition, the interactions between CB and HSA may result both from the ionization states of several groups on both the CB and the amino acid side chains of the HSA. The results also directed the electrostatic interaction and hydrophobic interaction were the important factors could affect the binding mechanism.

## Acknowledgments

This study was supported by the National Science Council, Taiwan (NSC 96-2218-E-008-022).

## References

- Altintas, E. B. and A. Denizli, "Efficient Removal of Albumin from Human Serum by Monosize Dye-Affinity Beads," *J. Chromatogr. B*, 832, 216 (2006).
- Chen, L. Y., M. C. Wu, M. T. Chou, L. A. Kao, S. J. Chen, and W. Y. Chen, "Effects of Solute-Matrix Interaction on Monitoring the Conformational Changes of Immobilized Proteins by Surface Plasmon Resonance Sensor," *Talanta*, 67, 862 (2005).
- Christina, B., Y. Qiuming, S. Chen, C. Y. Lee, H. Jifi, S. Y. Sinclair, and J. Shaoyi, "Surface Functionalization for Self-Referencing Surface Plasmon Resonance (SPR) Biosensors by Multi-Step Self-Assembly," *Sens. Actuator B-Chem.*, 90, 22 (2003).
- David, A. J., K. L. Elzbieta, C. P. Robert, and N. Hiroko, "Vesicular Properties of Stereoisomeric Surfactants," *Langmuir*, 12, 5803 (1996).
- Galina, Y. and P. Dimo, "Proteins at Fluid Interfaces: Adsorption Layers and Thin Liquid Films," *Adv. Colloid Interface Sci.*, 128–130, 159 (2006).
- Handan, Y., D. Erol, G. Ömer, and D. Adil, "Cibacron Blue F3GA Incorporated Poly( $\gamma$ -methylmethacrylate) Beads for Albumin Adsorption in Batch System," *Colloid Surf. A-Physicochem. Eng. Asp.*, 223, 185 (2003).
- Hua, L. N. and L. M. Zhu, "Adsorption of Papain with Cibacron Blue F3GA Carrying Chitosan-Coated Nylon Affinity Membranes," *Int. J. Biol. Macromol.*, 40, 261 (2007).
- Kassab, A., H. Yavuz, M. Odabas, and A. Denizli, "Human Serum Albumin Chromatography by Cibacron Blue F3GA-Derived Microporous Polyamide Hollow-Fiber Affinity Membranes," *J. Chromatogr. B*, 746, 123 (2000).
- Lewis, E. J., L. G. Hunsicker, and W. R. Clarke, "Renoprotective Effect of the Angiotensin-Receptor Antagonist Irbesartan in Patients with Nephropathy Due to Type 2 Diabetes," *N. Engl. J. Med.*, 345, 851 (2001).
- Lièvre, M., M. Marre, and G. Chatellier, "The Non-Insulin-Dependent Diabetes, Hypertension, Microalbuminuria or Proteinuria, Cardiovascular Events, and Ramipril (DIBHYCAR) Study Design. Organization, and Patient Recruitment," *Controlled Clin. Trials*, 21, 383 (2000).
- Martins, M. C., N. Esmaeel, D. R. Buddy, and A. B. Mario, "Albumin Adsorption on Cibacron Blue F3GA Immobilized onto Oligo(ethylene glycol)-Terminated Self-Assembled Monolayers," *J. Mater. Sci.-Mater. Med.*, 14, 945 (2003).
- Nan, Y., S. Xiaodi, T. Vinalia, and K. Wolfgang, "Evaluation of Two- and Three-Dimensional Streptavidin Binding Platforms for Surface Plasmon Resonance Spectroscopy Studies of DNA Hybridization and Protein-DNA Binding," *Biosens. Bioelectron.*, 22, 2700 (2007).
- Ottavio, G., P. Giuseppe, C. Aldo, C. Lorella, L. Amalia, N. Monica, C. Mauro, R. Loredana, and N. Renzo, "Which Method for Quantifying "Microalbuminuria" in Diabetics?" *Acta Diabetol.*, 28, 239 (1992).
- Pagana, K. D. and T. J. Pagana, *Mosby's Manual of Diagnostic and Laboratory Tests*, 3rd ed., Mosby Elsevier, St. Louis, USA (2006).
- Pantelis, A. S. and L. B. George, "Microalbuminuria and Chronic Kidney Disease as Risk Factors for Cardiovascular Disease," *Nephrol. Dial. Transplant.*, 21, 2366 (2006).
- Shengfu, C., L. Lingyan, L. B. Christina, and J. Shaoyi, "Controlled Chemical and Structural Properties of Mixed Self-Assembled Monolayers of Alkanethiols on Au(111)," *Langmuir*, 16, 9287 (2000).
- Sosnovsky, G. and P. Bell, "In the Search for New Anticancer Drugs. 29. A Study on the Correlation of Lipophilicities, Ionization Constants and Anticancer Activities of Aminoxy Labeled Tera Congeners," *Life Sci.*, 62, 639 (1998).

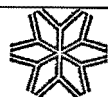


Spyridon, K., L. Ioannis, K. Ilias, I. Georgios, K. Theofanis, K. Athanasios, I. Konstantinos, T. Nikolaos, and A. Lambros, "Microalbuminuria: A Strong Predictor of 3-Year Adverse Prognosis in Nondiabetic Patients with Acute Myocardial Infarction," *Am. Heart J.*, 149, 840 (2005).

Stephan, M. C. B., V. M. David, and R. E. Melvin, "Determination of pKa Values of Organic Bases in Aqueous Acetonitrile Solutions Using Capillary Electrophoresis," *J. Chromatogr. A*, 71, 1004 (2003).

Ying, S., B. Yuping, S. Daqian, L. Xiaozhou, W. Liyang, and Z. Hanqi, "Design and Performances of Immunoassay Based on SPR Biosensor with Magnetic Microbeads," *Biosens. Bioelectron.*, 23, 473 (2007).

Zuwei, M., M. Kotaki, and R. Seeram, "Immobilization of Cibacron Blue F3GA on Electrospun Polysulphone Ultra-Fine Fiber Surfaces Towards Developing an Affinity Membrane for Albumin Adsorption," *J. Membr. Sci.*, 282, 237 (2006).



Contents lists available at ScienceDirect

## Colloids and Surfaces A: Physicochemical and Engineering Aspects

journal homepage: [www.elsevier.com/locate/colsurfa](http://www.elsevier.com/locate/colsurfa)

ELSEVIER



## Fabricating ordered porous monolayers from colloidal monolayer and multilayer

Ting Zhang<sup>a</sup>, Jun Qian<sup>a</sup>, Xinlin Tuo<sup>b,\*</sup>, Jun Yuan<sup>a</sup>, Xiaogong Wang<sup>b</sup><sup>a</sup> Electron Microscope Laboratory, National Centre for Electron Microscopy, Laboratory for Advanced Materials, School of Materials Science and Engineering, Tsinghua University, Beijing 100084, People's Republic of China<sup>b</sup> Department of Chemical Engineering, Laboratory for Advanced Materials, School of Materials Science and Engineering, Tsinghua University, Beijing 100084, People's Republic of China

## ARTICLE INFO

## Article history:

Received 4 June 2008

Received in revised form 21 October 2008

Accepted 9 November 2008

Available online 21 November 2008

## Keywords:

Colloidal monolayer and multilayer

Ordered porous film

Structure inversion

Template

## ABSTRACT

Both of the PSMA colloidal monolayer and multilayer were transformed to ordered porous monolayers in large-scale through selective solvent treatment. The pore formation is an *in situ* structure inversion process and the core-shell-like structure of PSMA colloid plays a critical role in pore formation and stabilization. The ordered porous polymer films, prepared by this method, can be used as a template for fabricating metal dot-arrays with large areas.

© 2008 Elsevier B.V. All rights reserved.

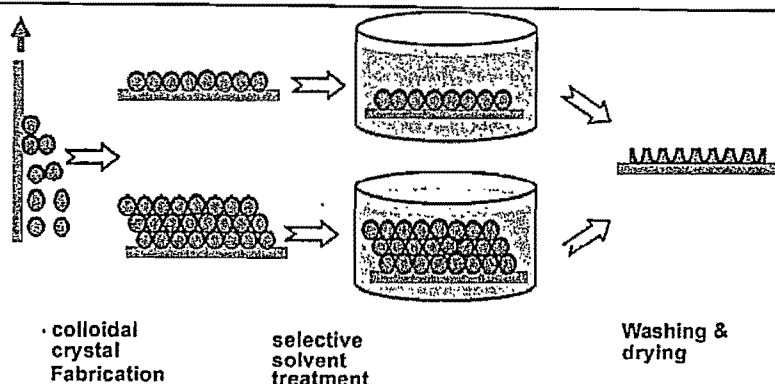
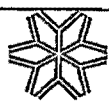
## 1. Introduction

Two-dimensional (2D) ordered micro/mesoporous polymer films have attracted considerable attention for their applications in various areas such as catalysis [1], photonic band-gap materials [2], surface-enhanced Raman spectroscopy (SERS) [3], cell cultures [4], high-density magnetic or optical information storage [5,6]. The method using colloidal monolayers as templates has been widely used in the creation of various 2D micro/mesoporous structures [7]. Typically, the ordered porous films are fabricated by the infiltration method [8]. In the process, the voids between colloidal spheres are infiltrated with sol-gel or polymeric precursors. When the precursors are solidified, the porous films can be obtained by removing the colloidal templates through wet-etching or thermal decomposition. However, the infiltration method is difficult to create the pores in diameter much smaller than the colloids. Recently, an alternative method based on the *in situ* structure inversion has been developed [9–12]. In a typical process, the dual-component colloid was converted to porous structure through thermal sintering or solvent extraction of the soluble component [10]. However, the colloids with specially designed structure limit the wide applications of this method and multi-step treatment would inevitably increase the number of defects in the final porous structure. There-

fore, it is highly desirable to develop this method in popularity and simplicity.

In this paper, we report a simple route to fabricate the ordered porous monolayer in large-scale based on the *in situ* structure inversion of a dual-component colloid. This method is also effective to transfer the colloidal multilayer as well as monolayer into porous monolayer. The highly monodispersed poly(styrene-co-methacrylic acid) (PSMA) colloids are used as the candidate. PSMA colloids, which contain styrene (St) and methacrylic acid (MAA) units, can be easily synthesized with high monodispersity (size dispersity much less than 5%) by surfactant-free emulsion polymerization. In this case, PSMA colloids are endowed with "core-shell"-like structure in characteristic with St rich in core and MAA rich in hydrated shell [13]. The strategy of this method is shown in Scheme 1. First, the highly monodispersed PSMA colloids self-assemble into colloidal crystal (monolayer or multilayer) on pretreated silicon surface. Second, the colloidal crystal is orientedly dipped into a selective solvent (for example of toluene), which is good solvent for polystyrene (PS) units and poor solvent for poly(methacrylic acid) (PMAA) units, and treated for a short (for monolayer) or long (for multilayer) time to fulfill the colloidal structure inversion. In this stage, the selective solvent initiates the change of colloidal structure. Solvent extraction drives the PS units in the core removed or locationally rearranged, which leads to the pore formation. In addition, the weak interaction between the solvent and the PMAA units stabilizes the pore structure. In this way, the colloidal monolayer is directly transferred into ordered

\* Corresponding author. Tel.: +86 10 62784561; fax: +86 10 62796171.  
E-mail address: [tuoxl@mail.tsinghua.edu.cn](mailto:tuoxl@mail.tsinghua.edu.cn) (X. Tuo).



Scheme 1. Fabrication of ordered porous monolayers through solvent-induced structure inversion.

porous monolayer, while the inversion of the colloidal multilayer undergoes a more complicated process, which will be detailed in following parts. Finally, the formed porous structure is quickly fixed by washing with another solvent, such as acetone, to remove the selective solvent and drying under air stream or nitrogen gas.

## 2. Experimental details

### 2.1. Colloidal synthesis and characterization

Mono-dispersed PSMA colloids were synthesized by typical surfactant-free emulsion polymerization. The St and MAA monomers were distilled before polymerization. The weight ratio of St to MAA was 9:1, and ammonium persulfate ( $(\text{NH}_4)_2\text{S}_2\text{O}_8$ ) was used as initiator. Polymerization was carried out in a 250 mL flask and the monomer mixture of 9 g St and 1 g MAA was added into 80 mL deionized water under stirring.  $\text{NaHCO}_3$  (0.24 g) was then added to the system to adjust the pH of emulsion. After that, the mixture was heated to 60 °C and 0.08 g  $(\text{NH}_4)_2\text{S}_2\text{O}_8$  in 20 mL water was added and the temperature was raised to 80 °C and the polymerization was carried out at the temperature for 10 h. For characterization, the resulted latex was collected by filtration, dialyzed and dried.

### 2.2. Preparation of colloidal monolayer and multilayer.

Colloidal monolayers on silicon wafer surface were prepared using vertical deposition method. As substrates, *N*-doped silicon (100) wafers were immersed in the mixture of  $\text{H}_2\text{SO}_4/\text{H}_2\text{O}_2$  (98% $\text{H}_2\text{SO}_4$ :30% $\text{H}_2\text{O}_2$  = 7:3, v/v) for 8 h at room temperature, then were ultrasonic treated in acetone, ethanol and deionized water respectively for three times before use. The initial colloidal emulsion was dialyzed with a large amount of deionized water and was diluted to 1 wt%. The silicon wafers were vertically dipped in the colloidal solution and the solution was slowly sucked out through a syringe. By controlling the decreasing velocity of the liquid surface level of the solution, colloidal monolayers or multilayer formed on silicon wafer surfaces. The formed colloidal crystals were vacuum-dried at 30 °C for 12 h before further experiments.

### 2.3. Porous film formation

The silicon wafers with the colloidal crystals on the surfaces were horizontally placed in toluene at room temperature for controllable periods. Then the substrates were taken out

with air stream and under vacuum at 30 °C for 12 h for further characterization.

### 2.4. Fabrication of Ni dot arrays

Porous templates were treated in a SE reactive ion etching machine with oxygen at 60 sccm, 10–2 Torr and 30 W for 10 s. After then Ni metal was deposited on templates, the porous templates were removed by ultrasonication in toluene for 15 min.

### 2.5. Characterization

Z-average diameters and size distributions of the latex particles were measured with dynamic laser light scattering (Zetasizer 3000 HS, Malvern Instruments Ltd., equipped with a 633 nm light source and detector angle is 90°). The surface morphology of colloidal monolayer and porous film were imaged with a scanning electron microscope (JEOL FESEM 6301) operated with an accelerating voltage of 5 kV. The samples were previously coated with thin gold layers before SEM measurements. Atomic force microscopic (AFM) images were recorded in the tapping mode with a scanning probe microscope (IIIa, Digital Instruments). Nuclear magnetic resonance ( $^1\text{H}$  NMR) spectra in chloroform- $d_3$  ( $\text{CDCl}_3$ ) were recorded on a JEOL JNM-ECA600 NMR spectrometer. The dialyzed latex solution was dried to collect the PSMA polymer for NMR measurement. The molar fraction of carbon and oxygen elements on the colloidal multilayer surface and porous film was measured by X-ray photoelectron spectroscopy (XPS) (PHI Quantera SXM, Scanning X-ray Microprobe). The contact angles of water on the colloidal multilayer surface and porous film were measured with the standard sessile drop technique by using a Dataphysics contact angle meter OCA-20. A water drop (2  $\mu\text{L}$ ) was made on the tip of a syringe and placed on a surface by moving the sample stage vertically until contact was made between the water drop and the surface. An image of the droplet was taken through a CCD camera and enlarged on computer screen. Contact angles were obtained by using the equipped software based on Young–Laplace fitting method. The contact angles reported in this paper are advancing contact angles. The pH value of the latex solution was measured by an acidimeter (PHS-25C, Kangyi Corp., China).

## 3. Results and discussion

Fig. 1(a) shows a typical scanning electron microscopy (SEM) image of the colloidal monolayers on silicon wafers. It can be seen that the colloids self-assembled into a hexagonal-close-packed 2D lattice. The average colloidal diameter was measured as 290 nm

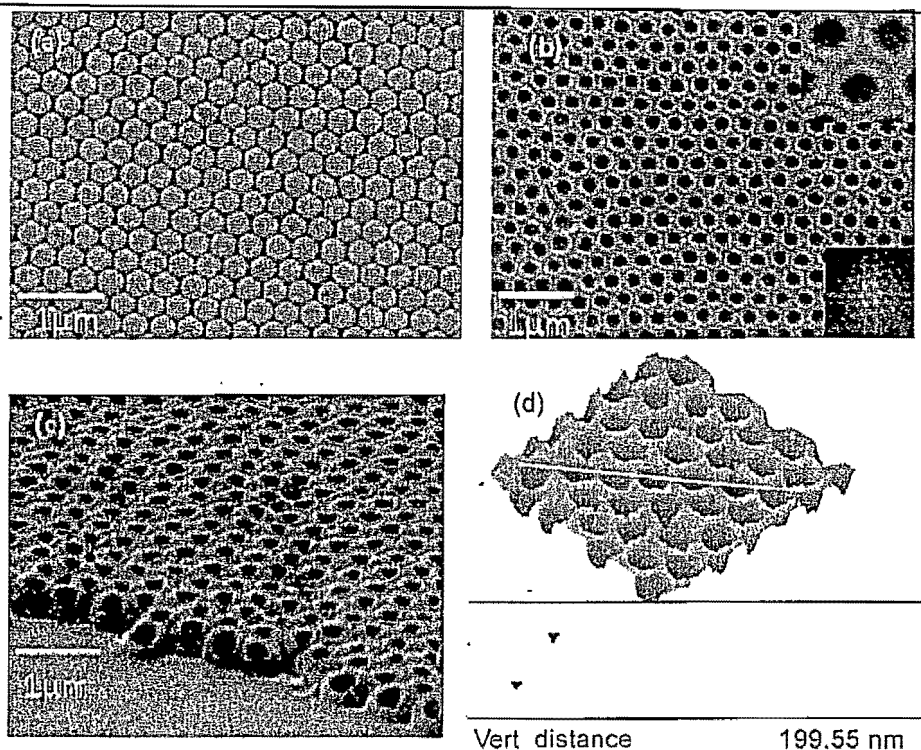
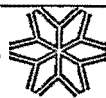


Fig. 1. (a) SEM image of the colloidal monolayer; (b) the porous monolayer image from top-view; (c) the porous monolayer image from side view; and (d) 3D AFM image of the porous monolayer and the depth profile of a pores line.

covered the supporting surface for about several square centimeters without apparent macroscopic defects.

The colloidal monolayer was directly transferred to ordered porous films by dipping in selective solvent, toluene. Fig. 1(b) shows a SEM image of the porous films, which were obtained by horizontally placing the monolayer-covered substrates in toluene for 40 s at room temperature. The pore width is 210 nm in average, which is less than the colloidal diameter, and the average center-to-center distance between the pores is about 290 nm, which indicates no obvious shrinkage occurred during the porous structure formation. The inserted Fourier transformation of the porous pattern reveals that the high periodicity of the porous films and large-scale porous monolayer could be easily obtained by this method (Figure S1, Supporting Information)[14]. An interesting observation from the other inserted image is that every pore has a distinguishable ring to be differed from each other (Figure S2, Supporting Information) [14], which indicates that the PMAA rich shell is strong enough to stabilize the pore structure. Fig. 1(c) gives a SEM image of the porous monolayer edge. The faultless round walls of the marginal pores indicate that the pore formation initiates from the colloidal centres instead of the voids between the colloids. In addition, the unruined porous wall further demonstrates the stabilization of the PMAA rich shell during porous structure formation. Fig. 1(d) shows a 3D atomic force microscopy (AFM) image of part of the porous films and the depth profile of one line of the pores. The average pore depth is near 200 nm, which shows that the pores almost penetrate the films and are deep enough for mask applications.

The colloidal multilayer undergoes a more complicated process in the porous monolayer fabrication. Experimentally, when a colloidal multilayer consisting of three monolayers (see Figure S3, Supporting Information) [14] was treated in toluene for short time (40 s), only the outmost layer was transferred into porous structure (Fig. 2a), which is similar with the colloidal monolayer. However, when treated with toluene for longer time (60–70 s), the inner col-

loids were gradually transferred into pores and the outmost porous film was gradually ruined (Fig. 2b) and finally removed by solvent (Fig. 2c). When the toluene treatment time reached 90 s, only the innermost layer was left and transferred into porous monolayer (Fig. 2d). Although the extract process is not clear, it is believed that the outer layers of the multilayer were layer-by-layered peeled off and the last layer was left. It is noteworthy that at the final stage PMAA units play an important role in the side-wall stabilization. PMAA units maintain the pore structure in toluene for longer time than PS based on their poor interaction with toluene and strong interaction with hydrated silicon surface. Therefore, the outlayers could be cleaned away without any remains, which enables the fabrication of the porous monolayer from colloidal multilayer.

To investigate the mechanism of the pore formation, we treated the PSMA colloidal monolayers with toluene for different time and imaged the structure variation with SEM. Fig. 3 gives four typical structure images during the pore formation when the colloidal monolayers were treated with toluene for about 10 s, 25 s, 60 s and 75 s, respectively. When the colloidal monolayer was treated for 10 s, the colloids conglutinated each other and most of the voids within colloids disappeared, several colloids even cracked (Fig. 3a). When the colloidal monolayer was treated for 25 s, porous structure appeared (Fig. 3b). Prolonging the treating time to 60 s, the pore was extended in width and depth and a few of the pores were even opened in the joint area (Fig. 3c). When the colloidal monolayer was treated for even longer time (75 s), the pores were severely ruined while the remains nevertheless outlined the porous structure, and some isolated porous walls could maintain their integrity (Fig. 3d).

The difference of the surface properties and surface elements between the colloidal monolayer and the obtained porous film were studied to further examine the rearrangement of the polymeric units. As have been reported by several other researchers that not all of the methacrylic acid could be incorporated into the

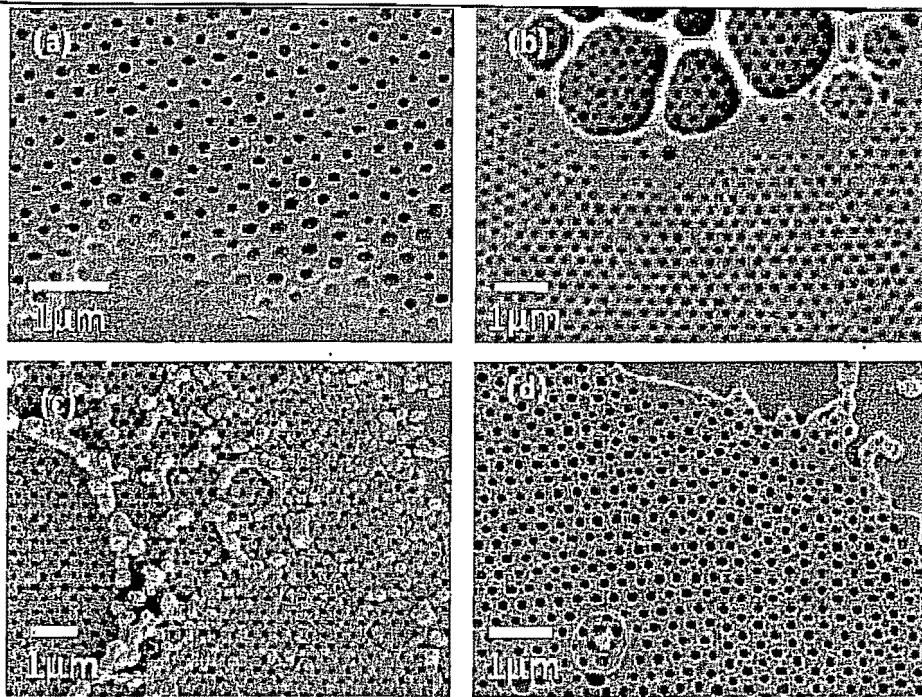


Fig. 2. (a) SEM image of colloidal multilayer with porous structure in outmost layer; (b) SEM image of colloidal multilayer with porous structure in the outmost and sub-layer; (c) SEM image of partially ruined porous structure in outmost layer; and (d) SEM image of porous monolayer.

latexes in the process of emulsion polymerization for methacrylate ion produced substantial amounts of water-soluble polyelectrolyte [15], we measured the actual weight ratio of St and MAA units in latex.  $^1\text{H}$  NMR spectroscopy was used to measure the bulk compositions of the copolymer latex and the result is shown in Figure S4 (see Supporting Information) [14]. The peaks at  $\delta = 6.20\text{--}7.10$  ppm and  $\delta = 0.85$  ppm are contributed to the hydrogens of phenyl ring

and methyl group, respectively. And consequent calculation reveals that the weight ratio of the polymerized St and MAA units was about 13:1. Compared to the feeding weight ratio of St:MAA = 9:1 in our experiment, we can see that not all of the hydrophilic MAA (methacrylic acid) units were polymerized into latex and the average molar contents of C and O elements is calculated to be 91.5% and 8.5%, respectively. In addition, the molar contents of C and O

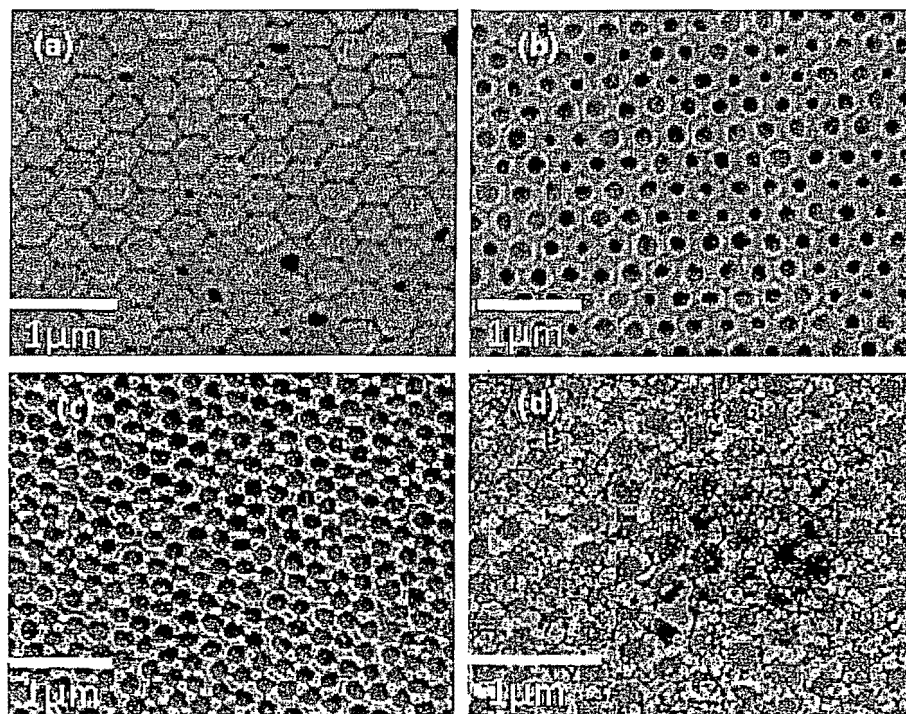


Fig. 3. SEM images of the surface morphologies when the colloidal monolayer was treated with toluene for (a) 10 s, (b) 25 s, (c) 60 s and (d) 75 s.

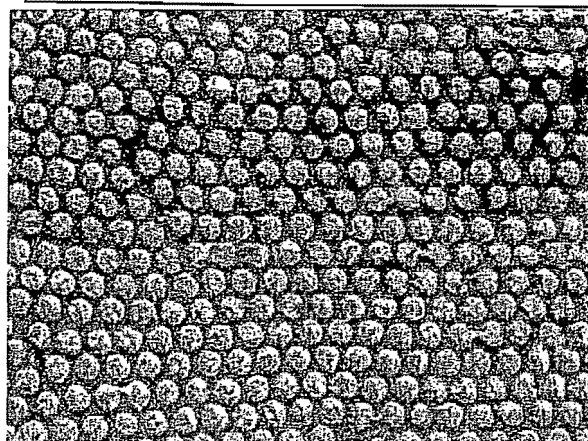
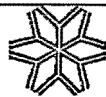


Fig. 4. SEM images of Ni dot arrays with top view.

elements on colloid surface were measured by XPS to be 81.62% and 18.38%. Moreover, pH measurement of the dialyzed latex solution showed that the latex solution was acidic (pH is about 5.5). All these demonstrated the MAA rich-in-shell structure of the colloids. When the colloid monolayer changed to be porous film, the molar contents of C and O elements on surface were measured to be 91.42% and 8.58% (Figure S5, Supporting Information) [14]. Obviously, the oxygen content at the surface of the porous films decrease. In addition, the porous film is more hydrophobic than that of the colloidal monolayer. The contact angles of colloidal monolayer and porous films are about  $10^\circ$  and  $93.1^\circ$ , respectively.

All the above results indicate that the porous monolayers are formed through a solvent-induced structure inversion. As previously reported in some literatures [13,15], the PSMA colloid polymerized with surfactant-free emulsion polymerization has a core-shell-like structure. Before solvent treatment, the PMAA units are rich in the colloidal shell and most PS units are in the colloidal core. When the colloids were treated with toluene, a good solvent for PS, the PS-rich cores were swollen and the colloids gradually conglutinated with each other and resulted in a "flat" film. This transformation was also observed when the colloidal arrays were annealed under toluene vapour. When the film was further exposed to toluene, the PS-rich segments moved out of the core region. Part of them were taken off and the rest were driven by surface tension not only to form an interface layer between the solvent and the PMA-rich segments, but also to fill the gaps in the original interstitial sites for its own surface energy minimization. Due to the shrinkage of the PMAA-rich segments in the solvent, the St-rich surface further adjusts morphology to form the rim of the pores. In short, the solvent dissolving effect leads the PS units to be extracted and fill in the voids, and the poor interaction of solvent with PMAA units makes the shell-rich PMAA units *in situ* stabilized. Based on this kind of collaboration, the PSMA colloidal monolayer completes its structure inversion. As to the colloidal multilayer, it is believed that the colloidal structure inversion is the same as that of the colloidal monolayer although the exact process of the layer-by-layered peeling off needs further study.

The ordered porous polymer films, prepared by this method, can show applications in diversified areas. As an example of the applications, the ordered porous films were used as a template to fabricate Ni dot-arrays. Fig. 4 shows the Ni arrays fabricated by using the polymeric template, which was prepared with a 290 nm St-co-MA colloidal crystals. In the process, the porous template was first treated with reactive ion etching (RIE) to remove the thin bottom layer at the deep end of the pores. Ni was then deposited by vac-

uum evaporation through the ordered pores. After ultrasonically washing in toluene, the polymeric template was removed and the Ni dot-arrays were formed on the substrate. The surface coverage by the metallic elements is high at the unit density. This is important for applications such as plasmonics and information storage, where the readout signal can be maximized.

#### 4. Conclusion

In conclusion, both of the PSMA colloidal monolayer and multilayer could be transformed to ordered porous monolayers in large-scale through selective solvent treatment. The pore formation is an *in situ* structure inversion process and the core-shell structure of PSMA colloid plays a critical role in pore formation and stabilization. The ordered porous polymer films, prepared by this method, show great applications in diversified areas, such as a template for fabricating mental dot-arrays, nanowire-arrays, which contributes to the potential application in storage, catalysis, and batteries.

#### Acknowledgments

This work was supported by NSFC under project (50303008) and MOST under project (2002AA302103).

#### Appendix A. Supplementary data

Supplementary data associated with this article can be found, in the online version, at doi:10.1016/j.colsurfa.2008.11.022.

#### References

- [1] S.I. Matsushita, T. Miwa, D.A. Tryk, A. Fujishima, *Langmuir* 14 (1998) 6441–6447.
- [2] A. Birner, U. Gruning, S. Ottow, A. Schneider, F. Müller, V. Lehmann, H. Föll, U. Gösele, *Phys. Status Solidi A* 165 (1998) 111–117.
- [3] (a) P.M. Tessier, O.D. Velev, A.T. Kalambur, J.F. Rabolt, A.M. Lenhoff, E.W. Kaler, *J. Am. Chem. Soc.* 122 (2000) 9554–9555;  
(b) P.M. Tessier, O.D. Velev, A.T. Kalambur, *Adv. Mater.* 13 (2001) 396–400.
- [4] T. Tatsuma, A. Ikezawa, Y. Ohko, T. Miwa, T. Matsue, A. Fujishima, *Adv. Mater.* 12 (2000) 643–646.
- [5] (a) S.H. Sun, C.B. Murray, D. Weller, L. Folks, A. Moser, *Science* 287 (2000) 1989–1992;  
(b) P.W. Wu, L.Q. Peng, X.L. Tuo, X.G. Wang, J. Yuan, *Nanotechnology* 16 (2005) 1693–1696.
- [6] (a) B.J. Siwick, O. Kallina, E. Kumacheva, R.J.D. Miller, J.J. Noolandi, *Appl. Phys.* 90 (2001) 5328–5334;  
(b) H.H. Pham, I. Goirevich, J.K. Oh, J.E.N. Jonkman, E. Kumacheva, *Adv. Mater.* 16 (2004) 516–520.
- [7] (a) Y. Li, W.P. Cai, G.T. Duan, *Chem. Mater.* 20 (2008) 615–624;  
(b) Y. Wang, U. Gösele, M. Steinhart, *Chem. Mater.* 20 (2008) 379–381;  
(c) A.Y. Lo, S.J. Huang, W.H. Chen, Y.R. Peng, C.T. Kuo, S.B. Liu, *Thin Solid Films* 498 (2006) 193–197.
- [8] (a) H. Míguez, F. Meseguer, C. Lopez, F. López-Tejeda, J. Sanchez-Dehesa, *Adv. Mater.* 13 (2001) 393–396;  
(b) M. Deutsch, Y.A.D. Vlasov, J. Norris, *Adv. Mater.* 12 (2000) 1176–1180;  
(c) F.Q. Sun, W.P. Cai, Y. Li, B.Q. Cao, Y. Lei, L.D. Zhang, *Adv. Funct. Mater.* 14 (2004) 283–287;  
(d) P. Jiang, M.J. McFarland, *J. Am. Chem. Soc.* 126 (2004) 13778–13786.
- [9] Y.B. Li, X.L. Tong, Y.N. He, X.G. Wang, *J. Am. Chem. Soc.* 128 (2006) 2220–2221.
- [10] D.K. Yi, D.Y. Kim, *Nano Lett.* 3 (2003) 207–211.
- [11] (a) Y.Y. Chen, W.T. Ford, N.F. Materer, D. Teeters, *J. Am. Chem. Soc.* 122 (2000) 10472–10473;  
(b) Y.Y. Chen, W.T. Ford, N.F. Materer, D. Teeters, *Chem. Mater.* 13 (2001) 2697–2704;  
(c) D.Q. Qin, S.S. Tan, S.H. Qin, W.T. Ford, *Langmuir* 20 (2004) 3145–3150.
- [12] M.J. Xue, W.T. Xiao, Z.J. Zhang, *Adv. Mater.* 20 (2008) 439–442.
- [13] (a) G.W. Ceska, *J. Appl. Polym. Sci.* 18 (1974) 2493–2499;  
(b) K. Sokota, T. Okaya, *J. Appl. Polym. Sci.* 21 (1977) 1025–1034;  
(c) C. Gajria, B.R. Vijayendran, *J. Appl. Polym. Sci.* 28 (1983) 1667–1684;  
(d) P.H. Wang, C.Y. Pan, *Colloid Polym. Sci.* 279 (2001) 98–103;  
(e) X. Chen, Z.C. Cui, Z.M. Chen, K. Zhang, G. Lu, G. Zhang, B. Yang, *Polymer* 43 (2002) 4147–4152.
- [14] See supporting information.
- [15] (a) S.T. Wang, G.W. Poehlein, *J. Appl. Polym. Sci.* 51 (1994) 593–604;  
(b) A.M. dosSantos, T.F. McKenna, J. Guillet, *J. Appl. Polym. Sci.* 65 (1997) 2343–2355;  
(c) P.H. Wang, C.Y. Pan, *Colloid Polym. Sci.* 280 (2002) 152–215.